Geophysical Research Letters

A new record of Atlantic sea surface salinity from 1896–2013 reveals the signatures of climate variability and long-term trends

Andrew R. Friedman[1], Gilles Reverdin[1], Myriam Khodri[1], and Guillaume Gastineau[1]

[1]Sorbonne-Universités, LOCEAN, CNRS/IRD/UPMC/MNHN, Paris, France

Corresponding authors: Gilles Reverdin (gilles.reverdin@locean-ipsl.upmc.fr), and Andrew R. Friedman (andrew.friedman@locean-ipsl.upmc.fr)

A formatted version of this paper was published by AGU. Copyright 2017, American Geophysical Union. *Geophysical Research Letters*, 44, 1866–1876. DOI:10.1002/2017GL072582.

Updated 24 March 2017

Key Points:

- Subpolar Atlantic surface salinity varies with the AMO, while low-latitude surface salinity lags by a decade and varies with the NAO
- Long-term surface salinity trends show freshening in the subpolar Atlantic and salinification in the tropical and subtropical Atlantic
- Northern tropical Atlantic surface salinity is negatively correlated with Sahel rainfall

Abstract

Sea surface salinity (SSS) is a major ocean circulation component and indicator of the hydrological cycle. Here we investigate an unprecedented Atlantic SSS compilation from 1896 to 2013 and analyze the main modes of SSS decadal variability. Using principal component analysis, we find that the low-latitude (tropical and subtropical) Atlantic and the subpolar Atlantic have distinct variability. Subpolar and low-latitude SSS are negatively correlated, with subpolar anomalies leading low-latitude anomalies by about a decade. Subpolar SSS varies in phase with the Atlantic Multidecadal Oscillation (AMO), whereas low-latitude SSS varies in phase with the North Atlantic Oscillation (NAO). Additionally, northern tropical SSS is anticorrelated with Sahel rainfall, suggesting that SSS reflects the Intertropical Convergence Zone latitude. The 1896–2013 SSS trend shows amplification of

the mean SSS field, with subpolar freshening and low-latitude salinification. The AMO and NAO have little effect on the long-term trend but contribute to the trend since 1970.

1 Introduction

Sea surface salinity (SSS) is a fundamental variable for ocean circulation and global climate. SSS results from the combined effects of evaporation (*E*), precipitation (*P*), land surface runoff, oceanic advection, vertical mixing, and from melting and freezing ice [*Yu*, 2011; *Vinogradova and Ponte*, 2013]. As large-scale SSS variations are thought to reflect the net surface freshwater flux (*E-P*), which is difficult to measure directly, SSS has been considered an indirect "ocean rain gauge" [*Schmitt*, 2008; *Terray et al.*, 2012; *Durack et al.*, 2013]. For instance, under global warming conditions, an intensification of the global hydrological cycle is projected due to the larger water vapor loading of the atmosphere, resulting in enhanced *E-P* in evaporative regions and reduced *E-P* in precipitative regions [*Held and Soden*, 2006]. Global SSS trends since the 1950s showing salinification in saltier regions and freshening in fresher regions provide evidence for such an intensification [*Helm et al.*, 2010; *Durack et al.*, 2012; *Skliris et al.*, 2014]. In the North Atlantic, SSS is of particular importance as it contributes to the density of water masses that take part in the upper branch of the Atlantic Meridional Overturning Circulation (AMOC) [*Kuhlbrodt et al.*, 2007], with well-established impacts on the Northern Hemisphere climate [*Paillard and Labeyrie*, 1994; *Stouffer et al.*, 2006] and on the ocean's capacity to store heat and carbon [*Joos et al.*, 1999; *Gruber et al.*, 2002]. Salinity variations also contribute to North Atlantic regional sea level change [*Steele and Ermold*, 2007; *Durack et al.*, 2014] and Atlantic marine biodiversity [*Lenoir et al.*, 2011].

Although the Atlantic is well sampled historically compared to other basins, continuous SSS time series beginning before the 1950s have been limited to small regions, e.g., the northeast subpolar gyre (SPG) [*Reverdin*, 2010]. This limited length of data has made it difficult to resolve decadal and multidecadal variability. For example, from the 1950s to the late 1990s, a freshening trend was reported in the subpolar North Atlantic [*Curry and Mauritzen*, 2005; *Boyer et al.*, 2005]. However, subpolar North Atlantic upper ocean salinity increased from the 1990s to the mid-2000s [*Holliday et al.*, 2008], resulting in slightly positive overall trends from 1950 to 2010 [*Durack and Wijffels*, 2010; *Skliris et al.*, 2014]. In the tropical and subtropical Atlantic, a salinification trend was reported from the 1950s to the late 1990s [*Curry et al.*, 2003; *Boyer et al.*, 2005; *Gordon and Giulivi*, 2008]. However, the North Atlantic Oscillation (NAO) experienced a positive trend during this period, which may have contributed to this salinification [*Curry et al.*, 2003]. In the tropical Atlantic, salinification was followed by freshening since the mid-1990s [*Grodsky et al.*, 2006; *Terray et al.*, 2012].

In this study, we present an unprecedented gridded SSS compilation spanning 118 years in the Atlantic north of 20°S, from 1896 to 2013. The increased temporal and spatial coverage allows us to resolve the major modes of SSS variability, which are linked to large-scale Atlantic climate variations. We also find long-term subpolar freshening and low-latitude salinification trends that are largely consistent with the expected impacts of global warming.

2 Data and Methods

2.1 Salinity Data

The SSS data are compiled from independently validated and bias-corrected in situ data sets from 1896 to 2013. The main data sources are previously described oceanographic research sections, weather ships, and ships-of-opportunity transects [*Reverdin et al.*, 1994; *Reverdin*, 1996; *Reverdin et al.*, 1997; *Alory et al.*, 2015]. These are complemented by

selected and validated upper level data from Nansen bottles and conductivity-temperature-depth casts from the World Ocean Database [*Boyer et al.*, 2013], Prediction and Research Moored Array in the Tropical Atlantic moorings [*Bourlès et al.*, 2008], and Argo float profiles from the Coriolis data set [*Gould et al.*, 2004; *Cabanes et al.*, 2013]. SSS is reported here as Practical Salinity Scale 1978 (PSS-78) [*Fofonoff*, 1985]. SSS uncertainties, including those related to collection and measurement errors [*Yu*, 2010; *Asher et al.*, 2014; *Anderson and Riser*, 2014; *Boutin et al.*, 2014], are discussed in the supporting information.

The source data are binned into 32 boxes of length scale 100–1000 km, chosen to be large enough to get some sampling through most of the period, but small enough that low-frequency (decadal) signals are coherent across each box. The boxes cover most of the Atlantic between 20°S and 70°N, excluding regions of large spatial variability which are insufficiently sampled: the Amazon and Orinoco freshwater plumes, the Gulf of Guinea, and north of the Gulf Stream. Monthly climatologies are constructed mainly based on the 1977–2013 reference period from *Reverdin et al.* [2007] (Figure S1 in the supporting information), for which we can most fully resolve the seasonal cycle over the entire domain.

The monthly climatologies are subtracted from individual measurements to obtain individual anomalies. In each gridbox, the individual anomalies are then median-averaged within each season (March–May, June–August, September–November, and December–February), and an error term is estimated (see the supporting information). For each season, an elementary 1-2-1 binomial filter is applied over successive years to reduce noise, and the filtered seasonal anomalies are centered to a 1896–2013 baseline (e.g., Figure 1a for March–May). To produce the yearly (March to February) time series, the 1-2-1 filtered seasonal time series are averaged, inversely weighted by their errors.

2.2 Climate Data

We investigate the linkages between SSS and two leading modes of North Atlantic climate variability: the NAO [*Hurrell et al.*, 2003] and the Atlantic Multidecadal Oscillation (AMO) [*Kerr*, 2000]. For the NAO, we use sea level pressure (SLP) from the NOAA-Cooperative Institute for Research in Environmental Sciences 20th Century Reanalysis, version 2c [*Compo et al.*, 2011]. The NAO is defined as the leading principal component (PC) of winter (December–March) mean SLP from 20° to 80°N, 90°W to 40°E [*Hurrell and Deser*, 2009]. A 1-2-1 binomial filter is applied to the yearly time series, similar to the SSS data. For the AMO, we use annual mean (March–February, similar to SSS) sea surface temperature (SST) from NOAA Extended Reconstructed Sea Surface Temperature, version 4 [*Huang et al.*, 2015]. The AMO is defined by regressing out global mean SST from the area-averaged North Atlantic SST anomaly (0–70°N, 7.5–75°W) [*Gastineau and Frankignoul*, 2015]; the SST time series are smoothed using a low-pass filter based on a combination of binomial filters, with a cutoff period of about 12 years [*Trenberth et al.*, 2007].

Additionally, we investigate the Sahel rainfall time series, constructed from the Global Historical Climatology Network Gridded Land Precipitation data set, version 2 [*Peterson and Vose*, 1997], from 1900 to 2013. The Sahel rainfall index is defined as the area-averaged rainfall anomaly from 10° to 20°N, 20°W to 10°E [*Mitchell*, 2015]. We also examine global mean surface temperature (GMST) from NASA Goddard Institute for Space Studies Surface Temperature Analysis [*Hansen et al.*, 2010; *GISTEMP Team*, 2016]. For both indices, we take the annual means from March–February and apply a 1-2-1 binomial filter.

3 Results

3.1 Regional SSS Variability

The (1-2-1 filtered) annual mean SSS standard deviation is shown in Figure 1b. To examine the main regions of coherent SSS variability, we apply empirical orthogonal function (EOF) analysis to the area-weighted SSS anomalies. The leading EOF (EOF1) accounts for 29% of the total variance and is well separated from EOF2 according to *North et al.* [1982] (Figure S2a). The leading principal component (PC1) is very highly correlated with area-averaged SSS from 20°S to 40°N ($r = 0.97$, $p < 0.01$), referred to as TATL (Figures S2b and S2d). The TATL spatial pattern (Figure 1c) is shown by the least squares regression onto the normalized time series, to indicate typical amplitudes. Hereafter, unless noted otherwise, correlation significance is evaluated by using a random-phase bootstrap test to account for serial autocorrelation [*Ebisuzaki*, 1997], using 12,000 iterations. The TATL pattern corresponds to a dipole structure with positive anomalies from 20°S to 40°N and with negative anomalies over the subpolar North Atlantic. The anomalies are significant ($p < 0.05$) over most of the gridboxes from 20°S to 40°N. The TATL time series (Figure 1e, bottom) experienced a pronounced salinification from 1975 to 1990, followed by a smaller decrease since 1995.

EOF2, which accounts for 16% of the total variance, is heavily localized in a few tropical Atlantic gridboxes, consisting of negative loadings in the large box from 5° to 15°N and positive loadings in the Antilles box (Figure S2c). As it is not well separated from EOF3 (12% of the total variance) and our focus is on large-scale regional variability, we do not discuss it further here.

Next, we focus on the northern North Atlantic. As EOF1 and EOF2 do not significantly project onto this region, we separately apply EOF analysis to the gridboxes north of 45°N. The leading EOF of the northern region (N-EOF1) accounts for 51% of the variance north of 45°N and is well separated from N-EOF2 (21% of the northern variance) [*North et al.*, 1982] (Figure S3a). N-PC1 is very highly correlated with area-averaged SSS from 45° to 62°N ($r = 0.985$, $p < 0.01$), referred to as NATL (Figures S3b and S3c). The NATL spatial pattern (Figure 1d) features a north-south dipole like TATL, but with the significant positive SSS slopes ($p < 0.05$) north of 45°N. The NATL time series (Figure 1e, top) features a long-term gradual freshening, punctuated by pronounced freshening events around 1920, and from the late 1960s to the mid-1970s, known as the Great Salinity Anomaly (GSA) [*Dickson et al.*, 1988]. Following a partial recovery around 1980, there were two smaller GSA-type events in the 1980s and 1990s [*Belkin et al.*, 1998; *Belkin*, 2004].

Figure 1f shows the lagged correlation of linearly detrended NATL and TATL (Figure S4a). We note that detrending does not change the NATL and TATL centers of action (Figures S4b and S4c); hereafter, all lagged correlations are for linearly detrended time series. NATL and TATL are significantly anticorrelated ($p < 0.05$) when NATL leads TATL by about a decade, with the strongest correlation at lag − 12 ($p < 0.01$). The correlation switches sign when TATL leads NATL, with a maximum when TATL leads by a decade. However, it just barely reaches the ($p < 0.05$) significance threshold.

3.2 Relationship With Climate Variability

Here we examine the relationship of climatic modes and detrended SSS. The NAO and AMO time series are shown in Figure 2a. They are significantly anticorrelated ($p < 0.05$) when the AMO leads the NAO by a few years (Figure S5), as noted previously [*Peings and Magnusdottir*, 2014]. The lagged correlations of the NAO with TATL and NATL are shown

in Figure 2c. The NAO and TATL are significantly correlated ($p < 0.05$) within lag ± 2, most significantly ($p < 0.01$) at lag − 0. Conversely, the NAO and NATL are not significantly correlated, although the coefficient has a local minimum at lag − 0. Figure 2b shows the spatial projection of SSS onto the NAO at lag − 0. It features a dipole pattern with positive slopes south of 45°N and negative slopes north of 45°N, albeit with limited statistical significance. Within NATL, there are significant negative correlations ($p < 0.05$) in the eastern SPG: the central eastern SPG (50°–55°N) is significant at lag − 0; the northeast SPG (55°–62°N) is significant at lag − 1 and lag − 2 (not shown), consistent with *Reverdin* [2010].

The significant correlation of the NAO and TATL presumably reflects the integrated influence of the NAO through wind-forced circulation and air-sea fluxes. The spatial pattern is consistent with surface freshwater fluxes, as the northward shift of storm tracks in positive NAO winters results in increased evaporation-precipitation (*E-P*) in the subtropics and decreased *E-P* in the SPG [*Hurrell and Deser*, 2009; *Stendardo et al.*, 2016]. In the tropics, the influence of the NAO onto SSS may reflect enhanced evaporation due to stronger trades and entrainment of saltier equatorial undercurrent water into the mixed layer [*Curry et al.*, 2003; *Mignot and Frankignoul*, 2004]. The NAO also drives significant changes in the gyre circulations [*Marshall et al.*, 2001; *Visbeck et al.*, 2003].

Figure 2d illustrates the NATL and TATL lagged correlations with the AMO. The AMO and NATL are significantly correlated ($p < 0.05$) within lag − 4 to lag + 3, most significantly ($p < 0.01$) at lag − 1. In contrast, the AMO and TATL are significantly negatively correlated ($p < 0.05$) when the AMO leads by around a decade. The lag − 0 spatial projection of the AMO onto SSS is shown in Figure 2e. All of the NATL gridboxes feature positive slopes, with the majority showing significant ($p < 0.05$) correlations. TATL is less consistent spatially, but there are negative slopes in the deep tropics, significantly ($p < 0.05$) from 5° to 20°N.

The significant covariability of NATL and the AMO is consistent with previous findings [*Polyakov et al.*, 2005; *Wang et al.*, 2010; *Zhang et al.*, 2013]. The AMO has not been found to have a strong signature on SPG rainfall [*Alexander et al.*, 2014]; rather, the NATL relationship is indicative of a net increase of the northward transport of saline waters into the SPG [*Hátún et al.*, 2005; *Häkkinen et al.*, 2011]. This may also suggest a role for the AMOC in the AMO, as proposed in theoretical and modeling studies, where an AMOC intensification is associated with an increase of warm and saline water into the subpolar region [e.g., *Delworth et al.*, 1993; *Vellinga and Wu*, 2004; *Latif et al.*, 2004; *Knight et al.*, 2005].

The negative correlation of the AMO and northern tropical SSS suggests a connection with the Atlantic Intertropical Convergence Zone (ITCZ), whose latitudinal displacement—as reflected in Sahel rainfall—is linked to the AMO [*Zhang and Delworth*, 2006; *Ting et al.*, 2011]. To explore this connection, we examine the Sahel rainfall time series (Figure 2f, top). The lag − 1 spatial projection of SSS onto Sahel rainfall (Figure 2g) features positive slopes in the northeast Atlantic and significant negative slopes in the tropical Atlantic adjacent to the Sahel. The area average of the three strongly negative boxes from 55° to 20°W, 5° to 20°N (referred to as NTROP) is shown in Figure 2f (bottom). NTROP is significantly negatively correlated ($p < 0.05$) with Sahel rainfall from lag − 3 to lag + 1, most significantly ($p < 0.01$) at lag − 2 (Figure 2h). The significant negative relationship may indicate a direct influence of the marine ITCZ on SSS via precipitation fluxes. It may also reflect evaporation or entrainment mechanisms, which were found to be dominant factors for tropical Atlantic SSS over recent decades where satellite ocean precipitation estimates are available [*Grodsky et al.*, 2006].

3.3 Long-Term Trends and Pattern Amplification

We investigate SSS trends over the entire record from 1896 to 2013 and from 1970 to 2013, the recent period of relatively continuous GMST increase [*Cahill et al.*, 2015]. Figure 3a shows the NATL and TATL time series from Figure 1e with the 1896–2013 and 1970–2013 trends. TATL has an 1896–2013 salinification trend of 0.040 ± 0.031 PSS-78 per 50 years (slope ± 95% confidence interval (CI); trend CIs are constructed by resampling the trend residuals using the random-phase bootstrap described earlier). NATL has an 1896–2013 freshening trend of −0.042 ± 0.020 PSS-78 per 50 years. The 1896–2013 spatial trend pattern (Figure 3c) shows coherent signs within the TATL and NATL regions—all NATL boxes show freshening, and all TATL gridboxes show salinification. The most positive trends are from 15° to 20°N, with the maximum salinification from 30° to 55°W (0.091 ± 0.037 PSS-78 per 50 years). The most negative trends are in the western SPG and Labrador Sea, with the maximum freshening within (30°–45°W, 50°–55°N): −0.089 ± 0.017 PSS-78 per 50 years.

Durack et al. [2012] characterize the intensification of the mean SSS field by regressing the zonal mean SSS trend onto the zonal mean SSS climatology; they term the slope the pattern amplification (PA) coefficient. Here we area average the 32 gridboxes into nine roughly zonal banded regions (black dashed lines in Figure 3c). The zonally aggregated trends verus climatologies (from Figure 1a) are depicted in Figure 3g, which shows a strong relationship between the trends and climatologies. The 1896–2013 slope, which we term the Atlantic PA, is 3.7 ± 2.9% per 50 years (slope ± 95% CI; Atlantic PA CIs are calculated as 1.96 × Atlantic PA slope standard errors; see the supporting information). Using the 1896–2013 GMST trend of 0.40 ± 0.12°C per 50 years, we can express the Atlantic PA as 9.1 ± 7.7 % per °C (slope ± 95% CI; see the supporting information).

For 1970–2013, both NATL (0.082 ± 0.050 PSS-78 per 50 years) and TATL (0.088 ± 0.099 PSS-78 per 50 years) have salinification trends. The spatial trend pattern (Figure 3e) shows strong positive trends in most of the basin, most significantly north of 15°N. There is also freshening from 5° to 20°N. The 1970–2013 Atlantic PA of 2.8 ± 7.5% per 50 years (Figure 3h) is smaller than 1896–2013. Dividing this by the 1970–2013 GMST trend of 0.87 ± 0.07°C per 50 years yields a scaled Atlantic PA of 3.2 ± 8.6 % per °C, substantially smaller than the 1896–2013 value.

3.4 Multiple Regression

The long-term trends may be convolved with the AMO and NAO influence described in section 3.2. As a first-order decomposition, we remove the lag − 0 fits of the AMO and NAO by using a multiple regression framework, similar to *Durack and Wijffels* [2010]:

$$SSS = B_1 NAO + B_2 AMO + \varepsilon \qquad (1)$$

where ε is the residual SSS, which includes a secular trend plus remaining variability (including AMO and NAO lagged responses). Equation (1) differs from the bivariate regressions in section 3.2 in that the variables are not detrended prior to the analysis. However, the 1896–2013 trends are not significant for either the NAO (0.11 ± 0.35 normalized units per 50 years) or the AMO (−0.016 ± 0.12°C per 50 years).

The residual NATL and TATL time series are shown in Figure 3b. Both have significant 1896–2013 trends: 0.036 ± 0.021 PSS-78 per 50 years (TATL) and −0.039 ± 0.014 PSS-78 per 50 years (NATL). The 1896–2013 residual trend pattern (Figure 3d) is very similar to the original trend pattern (Figure 3c) except for two fewer significant gridboxes. Figure 3i compares the residual zonal mean trends from Figure 3d versus the climatology. The 1896–

2013 residual Atlantic PA (3.3 ± 2.8% per 50 years) is about 10% smaller than observations. Applying equation (1) to GMST yields an 1896–2013 residual trend of 0.40 ± 0.10°C per 50 years; the 1896–2013 residual Atlantic PA scaled to this value is 8.3 ± 7.3 % per °C.

For 1970–2013, there is a significant trend in the AMO (0.46 ± 0.21°C per 50 years), though not the NAO (0.13 ± 1.4 normalized units per 50 years). As a result, the prominent regions where the trend signal is captured by the multiple regression are where the AMO fit is strong (Figure 2e). The residual 1970–2013 trend pattern (Figure 3f) shows a reversal of the freshening from 5° to 20°N, 55° to 25°W in Figure 3e, resulting in a more coherent TATL salinification. The 1970–2013 residual TATL trend (0.11 ± 0.069 PSS-78 per 50 years) is thus stronger than the original data. The residual NATL trend has weak freshening (–0.004 ± 0.073 PSS-78 per 50 years). SPG residual gridbox trends show reduced salinification, with some boxes showing freshening. Overall, the residual pattern is more consistent with the 1896–2013 trend. The 1970–2013 residual Atlantic PA of 6.7 ± 4.2% per 50 years (Figure 3j) is significant, unlike the original data. Scaling the residual Atlantic PA to the 1970–2013 residual GMST trend (0.77 ± 0.08°C per 50 years) yields 8.7 ± 5.5 % per °C, which is much larger than the original 1970–2013 scaled PA, and similar to the 1896–2013 Atlantic PA estimate.

4 Discussion

In this study, we describe the leading variability in a new SSS record from 1896 to 2013. We find that subpolar SSS varies in phase with the AMO, whereas low-latitude SSS lags by about a decade and varies in phase with the NAO. An unresolved question is whether the decadal TATL lag reflects its local response (as the NAO lags the AMO) or a decadal lagged response to the AMO through the ocean circulation. In the latter case, the AMO may influence tropical SSS via the position of the ITCZ; the tropical anomalies could then be advected around the TATL region. In some climate models, this mechanism forms part of a larger feedback that explains AMOC variability: the tropical SSS anomalies eventually propagate northward, reaching the subpolar North Atlantic after several decades and weakening the AMOC [*Vellinga and Wu*, 2004; *Mignot and Frankignoul*, 2010]. Although the length of the SSS data set is too limited to clearly distinguish salinity advection from direct atmospheric forcing, the significant negative correlation of northern tropical SSS with Sahel rainfall is consistent with the first part of this feedback and opens questions for further research.

We also describe long-term subpolar freshening and low-latitude salinification trends, which project onto the mean SSS climatology. The 1896–2013 trend pattern is robust to removing the linear lag − 0 AMO and NAO fits through multiple regression. For 1970–2013, removing the AMO and NAO fits reverses the northern tropical Atlantic freshening and subpolar salinfication trends, resulting in much more significant Atlantic pattern amplification in the multiple regression residual than in the full data over this period. This Atlantic pattern amplification is consistent with the "rich-get-richer" paradigm of hydrological cycle intensification [*Held and Soden*, 2006] and increased atmospheric moisture transport from the low-latitude Atlantic to the Pacific [*Richter and Xie*, 2010]. Similar SSS spatial patterns have been shown in the 21st century and idealized simulations with enhanced *E-P* fluxes [*Stott et al.*, 2008; *Terray et al.*, 2012; *Durack et al.*, 2012].

Advective processes may also be very important for both the TATL salinification and NATL freshening trends. A potential contributor to the TATL salinification is Agulhas leakage, which is projected to have increased since the 1960s due to intensifying Southern Hemisphere westerlies [*Biastoch et al.*, 2015]. For NATL, there is an opposing balance between Arctic freshwater export—including GSA-type events—and northward flowing Atlantic water. Over

the past several decades, subpolar Atlantic and Arctic freshwater convergence have increased due to cryosphere melting and surface runoff [*Peterson et al.*, 2006; *Yang et al.*, 2016]. An opposing mechanism for NATL found in some model simulations is that northward advected Atlantic waters are becoming saltier, which would increase NATL salinity [*Latif et al.*, 2000; *Pardaens et al.*, 2008]. The 1896–2013 NATL freshening trend suggests that this latter process has not outweighed the decreased *E-P* fluxes and Arctic freshwater export, although it could account for the weaker trends in the eastern SPG and Norwegian Sea salinification. One caveat is that SSS does not directly indicate the net freshwater convergence, for which we would need the vertical integral (although the subpolar Atlantic winter mixed layer often extends hundreds of meters). Finally, an important question is whether the long-term NATL freshening indicates a century-long weakening of the AMOC, as suggested recently [*Rahmstorf et al.*, 2015]. Further sensitivity studies are needed to assess the potential reduction in deep convection implied by the subpolar SSS decrease.

Acknowledgments

A.R.F. was supported by the French National Research Agency under the program *Facing Societal*, *Climate and Environmental Changes* (MORDICUS project, grant ANR-13-SENV-0002). This study is a contribution to the French SSS observation service, which is supported by French agencies INSU/CNRS, IRD, CNES, and IPEV. We thank Elodie Kestenare and Gael Alory for contributing to the data validation and Juliette Mignot and Nicolas Lebas for valuable suggestions. Constructive feedback from two anonymous reviewers is highly appreciated. Support for the 20th Century Reanalysis Project version 2c data set is provided by the U.S. Department of Energy, Office of Science Biological and Environmental Research (BER), and by the NOAA Climate Program Office. The 20th Century Reanalysis v2c output and GHCN Gridded v2 precipitation data were provided by the NOAA/OAR/ESRL PSD, and the ERSST v4 data were provided by the NOAA NCEI. The SSS time series will be archived at the Laboratory of Studies on Spatial Geophysics and Oceanography: http://www.legos.obs-mip.fr/observations/sss/.

References

Alexander, M. A., K. Halimeda Kilbourne, and J. A. Nye (2014), Climate variability during warm and cold phases of the Atlantic Multidecadal Oscillation (AMO) 1871–2008, J. Mar. Syst., 133, 14–26, doi:*10.1016/j.jmarsys.2013.07.017*.

Alory, G., et al. (2015), The French contribution to the voluntary observing ships network of sea surface salinity, Deep Sea Res., Part I, 105, 1–18, doi:*10.1016/j.dsr.2015.08.005*.

Anderson, J. E., and S. C. Riser (2014), Near-surface variability of temperature and salinity in the near-tropical ocean: Observations from profiling floats, J. Geophys. Res. Oceans, 119, 7433–7448, doi:*10.1002/2014JC010112*.

Asher, W. E., A. T. Jessup, and D. Clark (2014), Stable near-surface ocean salinity stratifications due to evaporation observed during STRASSE, J. Geophys. Res. Oceans, 119, 3219–3233, doi:*10.1002/2014JC009808*.

Belkin, I. M. (2004), Propagation of the "Great Salinity Anomaly" of the 1990s around the northern North Atlantic, Geophys. Res. Lett., 31, L08306, doi:*10.1029/2003GL019334*.

Belkin, I. M., S. Levitus, J. Antonov, and S.-A. Malmberg (1998), "Great Salinity Anomalies" in the North Atlantic, Prog. Oceanogr., 41(1), 1–68, doi:*10.1016/S0079-6611(98)00015-9*.

Biastoch, A., J. V. Durgadoo, A. K. Morrison, E. van Sebille, W. Weijer, and S. M. Griffies (2015), Atlantic multi-decadal oscillation covaries with Agulhas leakage, Nat. Commun., 6, 10082, doi:*10.1038/ncomms10082*.

Bourlès, B., et al. (2008), The Pirata program: History, accomplishments, and future directions, Bull. Am. Meteorol. Soc., 89(8), 1111–1125, doi:*10.1175/2008BAMS2462.1*.

Boutin, J., N. Martin, G. Reverdin, S. Morisset, X. Yin, L. Centurioni, and N. Reul (2014), Sea surface salinity under rain cells: SMOS satellite and in situ drifters observations, J. Geophys. Res. Oceans, 119, 5533–5545, doi:*10.1002/2014JC010070*.

Boyer, T. P., S. Levitus, J. I. Antonov, R. A. Locarnini, and H. E. Garcia (2005), Linear trends in salinity for the World Ocean, 1955–1998, Geophys. Res. Lett., 32, L01604, doi:*10.1029/2004GL021791*.

Boyer, T. P., et al. (2013), World Ocean Database 2013, NOAA Atlas NESDIS 72, 209 pp., Silver Spring, Md., doi:*10.7289/V5NZ85MT*.

Cabanes, C., et al. (2013), The CORA dataset: Validation and diagnostics of in-situ ocean temperature and salinity measurements, Ocean Sci., 9(1), 1–18, doi:*10.5194/os-9-1-2013*.

Cahill, N., Rahmstorf, S., and Parnell, A. C. (2015), Change points of global temperature, Environ. Res. Lett., 10(8), 084002, doi:*10.1088/1748-9326/10/8/084002*.

Compo, G. P., et al. (2011), The Twentieth Century Reanalysis Project, Q. J. R. Meteorol. Soc., 137(654), 1–28, doi:*10.1002/qj.776*.

Curry, R., and C. Mauritzen (2005), Dilution of the northern North Atlantic Ocean in recent decades, Science, 308(5729), 1772–1774, doi:*10.1126/science.1109477*.

Curry, R., B. Dickson, and I. Yashayaev (2003), A change in the freshwater balance of the Atlantic Ocean over the past four decades, Nature, 426(6968), 826–829, doi:*10.1038/nature02206*.

Delworth, T., S. Manabe, and R. J. Stouffer (1993), Interdecadal variations of the thermohaline circulation in a coupled ocean-atmosphere model, J. Clim., 6(11), 1993–2011, doi:*10.1175/1520-0442(1993)006<1993:IVOTTC>2.0.CO;2*.

Dickson, R. R., J. Meincke, S.-A. Malmberg, and A. J. Lee (1988), The "Great Salinity Anomaly" in the northern North Atlantic 1968–1982, Prog. Oceanogr., 20(2), 103–151.

Durack, P. J., and S. E. Wijffels (2010), Fifty-year trends in global ocean salinities and their relationship to broad-scale warming, J. Clim., 23(16), 4342–4362, doi:*10.1175/2010JCLI3377.1*.

Durack, P. J., S. E. Wijffels, and R. J. Matear (2012), Ocean salinities reveal strong global water cycle intensification during 1950 to 2000, Science, 336(6080), 455–458, doi:*10.1126/science.1212222*.

Durack, P. J., Wijffels, S. E., and Boyer, T. P. (2013), Chapter 28—Long-term salinity changes and implications for the global water cycle, in International Geophysics, vol. 103, edited by S. M. G. G. Siedler, J. Gould and J. A. Church, pp. 727–757, Academic Press, Oxford, U. K. [Available at *http://www.sciencedirect.com/science/article/pii/B9780123918512000283*.]

Durack, P. J., Wijffels, S. E., and Gleckler, P. J. (2014), Long-term sea-level change revisited: The role of salinity, Environ. Res. Lett., 9(11), 114017, doi:*10.1088/1748-9326/9/11/114017*.

Ebisuzaki, W. (1997), A method to estimate the statistical significance of a correlation when the data are serially correlated, J. Clim., 10(9), 2147–2153.

Fofonoff, N. P. (1985), Physical properties of seawater: A new salinity scale and equation of state for seawater, J. Geophys. Res., 90, 3332–3342, doi:*10.1029/JC090iC02p03332*.

Gastineau, G., and C. Frankignoul (2015), Influence of the North Atlantic SST variability on the atmospheric circulation during the twentieth century, J. Clim., 28(4), 1396–1416, doi:*10.1175/JCLI-D-14-00424.1*.

GISTEMP Team (2016), GISS Surface Temperature Analysis (GISTEMP), NASA Goddard Institute for Space Studies, New York. [Available at *https://data.giss.nasa.gov/gistemp/*, dataset accessed 2016-12-14.]

Gordon, A., and C. Giulivi (2008), Sea surface salinity trends over fifty years within the subtropical North Atlantic, Oceanography, 21(1), 20–29, doi:*10.5670/oceanog.2008.64*.

Gould, J., et al. (2004), Argo profiling floats bring new era of in situ ocean observations, Eos Trans. AGU, 85(19), 179–184.

Grodsky, S. A., J. A. Carton, and F. M. Bingham (2006), Low frequency variation of sea surface salinity in the tropical Atlantic, Geophys. Res. Lett., 33, L14604, doi:*10.1029/2006GL026426*.

Gruber, N., C. D. Keeling, and N. R. Bates (2002), Interannual variability in the North Atlantic Ocean carbon sink, Science, 298(5602), 2374–2378, doi:*10.1126/science.1077077*.

Häkkinen, S., P. B. Rhines, and D. L. Worthen (2011), Warm and saline events embedded in the meridional circulation of the northern North Atlantic, J. Geophys. Res., 116, C03006, doi:*10.1029/2010JC006275*.

Hansen, J., R. Ruedy, M. Sato, and K. Lo (2010), Global surface temperature change, Rev. Geophys., 48, RG4004, doi:*10.1029/2010RG000345*.

Hátún, H., A. B. Sandø, H. Drange, B. Hansen, and H. Valdimarsson (2005), Influence of the Atlantic subpolar gyre on the thermohaline circulation, Science, 309(5742), 1841–1844, doi:*10.1126/science.1114777*.

Held, I., and B. Soden (2006), Robust responses of the hydrological cycle to global warming, J. Clim., 19(21), 5686–5699.

Helm, K. P., N. L. Bindoff, and J. A. Church (2010), Changes in the global hydrological-cycle inferred from ocean salinity, Geophys. Res. Lett., 37, L18701, doi:*10.1029/2010GL044222*.

Holliday, N. P., et al. (2008), Reversal of the 1960s to 1990s freshening trend in the northeast North Atlantic and Nordic Seas, Geophys. Res. Lett., 35, L03614, doi:*10.1029/2007GL032675*.

Huang, B., et al. (2015), Extended reconstructed sea surface temperature version 4 (ERSST.v4). Part I: Upgrades and intercomparisons, J. Clim., 28(3), 911–930, doi:*10.1175/JCLI-D-14-00006.1*.

Hurrell, J. W., and C. Deser (2009), North Atlantic climate variability: The role of the North Atlantic Oscillation, J. Mar. Syst., 78(1), 28–41, doi:*10.1016/j.jmarsys.2008.11.026*.

Hurrell, J. W., Y. Kushnir, G. Ottersen, and M. H. Visbeck (2003), An overview of the North Atlantic Oscillation, in The North Atlantic Oscillation: Climate Significance and Environmental Impact, vol. 134, pp. 1–35, AGU, Washington, D. C.

Joos, F., G.-K. Plattner, T. F. Stocker, O. Marchal, and A. Schmittner (1999), Global warming and marine carbon cycle feedbacks on future atmospheric CO2, Science, 284(5413), 464–467, doi:*10.1126/science.284.5413.464*.

Kerr, R. A. (2000), A North Atlantic climate pacemaker for the centuries, Science, 288(5473), 1984–1985, doi:*10.1126/science.288.5473.1984*.

Knight, J., R. Allan, C. Folland, M. Vellinga, and M. Mann (2005), A signature of persistent natural thermohaline circulation cycles in observed climate, Geophys. Res. Lett., 32, L20708, doi:*10.1029/2005GL024233*.

Kuhlbrodt, T., A. Griesel, M. Montoya, A. Levermann, M. Hofmann, and S. Rahmstorf (2007), On the driving processes of the Atlantic meridional overturning circulation, Rev. Geophys., 45, RG2001, doi:*10.1029/2004RG000166*.

Latif, M., E. Roeckner, U. Mikolajewicz, and R. Voss (2000), Tropical stabilization of the thermohaline circulation in a greenhouse warming simulation, J. Clim., 13(11), 1809–1813, doi:*10.1175/1520-0442(2000)013<1809:L>2.0.CO;2*.

Latif, M., et al. (2004), Reconstructing, monitoring, and predicting multidecadal-scale changes in the North Atlantic Thermohaline circulation with sea surface temperature, J. Clim., 17(7), 1605–1614, doi:*10.1175/1520-0442(2004)017<1605:RMAPMC>2.0.CO;2*.

Lenoir, S., G. Beaugrand, and É. Lecuyer (2011), Modelled spatial distribution of marine fish and projected modifications in the North Atlantic Ocean, Global Change Biol., 17(1), 115–129, doi:*10.1111/j.1365-2486.2010.02229.x*.

Marshall, J., H. Johnson, and J. Goodman (2001), A study of the interaction of the North Atlantic oscillation with ocean circulation, J. Clim., 14(7), 1399–1421, doi:*10.1175/1520-0442(2001)014<1399:ASOTIO>2.0.CO;2*.

Mignot, J., and C. Frankignoul (2004), Interannual to interdecadal variability of sea surface salinity in the Atlantic and its link to the atmosphere in a coupled model, J. Geophys. Res., 109, C04005, doi:*10.1029/2003JC002005*.

Mignot, J., and C. Frankignoul (2010), Local and remote impacts of a tropical Atlantic salinity anomaly, Clim. Dyn., 35(7–8), 1133–1147, doi:*10.1007/s00382-009-0621-9*.

Mitchell, T. (2015), Sahel Precipitation Index, Joint Institute for the Study of the Atmosphere and Ocean, Univ. of Washington, Seattle, doi:*10.6069/H5MW2F2Q*.

North, G. R., T. L. Bell, R. F. Cahalan, and F. J. Moeng (1982), Sampling errors in the estimation of empirical orthogonal functions, Mon. Weather Rev., 110(7), 699–706, doi:*10.1175/1520-0493(1982)110<0699:SEITEO>2.0.CO;2*.

Paillard, D., and L. Labeyrie (1994), Role of the thermohaline circulation in the abrupt warming after Heinrich events, Nature, 372(6502), 162–164, doi:*10.1038/372162a0*.

Pardaens, A., M. Vellinga, P. Wu, and B. Ingleby (2008), Large-scale atlantic salinity changes over the last half-century: A model–observation comparison, J. Clim., 21(8), 1698–1720, doi:*10.1175/2007JCLI1988.1*.

Peings, Y., and G. Magnusdottir (2014). Forcing of the wintertime atmospheric circulation by the multidecadal fluctuations of the North Atlantic Ocean, Environ. Res. Lett., 9(3), 034018, doi:*10.1088/1748-9326/9/3/034018*.

Peterson, T. C., and R. S. Vose (1997), An overview of the global historical climatology network temperature database, Bull. Am. Meteorol. Soc., 78(12), 2837–2849.

Peterson, B. J., J. McClelland, R. Curry, R. M. Holmes, J. E. Walsh, and K. Aagaard (2006), Trajectory shifts in the Arctic and subarctic freshwater cycle, Science, 313(5790), 1061–1066, doi:*10.1126/science.1122593*.

Polyakov, I. V., U. S. Bhatt, H. L. Simmons, D. Walsh, J. E. Walsh, and X. Zhang (2005), Multidecadal variability of North Atlantic temperature and salinity during the twentieth century, J. Clim., 18(21), 4562–4581, doi:*10.1175/JCLI3548.1*.

Rahmstorf, S., J. E. Box, G. Feulner, M. E. Mann, A. Robinson, S. Rutherford, and E. J. Schaffernicht (2015), Exceptional twentieth-century slowdown in Atlantic Ocean overturning circulation, Nat. Clim. Change, 5(5), 475–480, doi:*10.1038/nclimate2554*.

Reverdin, G. (1996), Upper ocean temperature and salinity sections in the South Atlantic in 1911, J. Geophys. Res., 101, 6361–6376, doi:*10.1029/95JC03374*.

Reverdin, G. (2010), North Atlantic subpolar gyre surface variability (1895–2009), J. Clim., 23(17), 4571–4584, doi:*10.1175/2010JCLI3493.1*.

Reverdin, G., D. Cayan, H. Dooley, D. Ellett, S. Levitus, Y. Dupenhoat, and A. Dessier (1994), Surface salinity of the North-Atlantic—Can we reconstruct its fluctuations over the last 100 years, Prog. Oceanogr., 33(4), 303–346, doi:*10.1016/0079-6611(94)90021-3*.

Reverdin, G., D. Cayan, and Y. Kushnir (1997), Decadal variability of hydrography in the upper northern North Atlantic in 1948–1990, J. Geophys. Res., 102, 8505–8531, doi:*10.1029/96JC03943*.

Reverdin, G., E. Kestenare, C. Frankignoul, and T. Delcroix (2007), Surface salinity in the Atlantic Ocean (30°S–50°N), Prog. Oceanogr., 73(3–4), 311–340, doi:*10.1016/j.pocean.2006.11.004*.

Richter, I., and S. Xie (2010), Moisture transport from the Atlantic to the Pacific basin and its response to North Atlantic cooling and global warming, Clim. Dyn., 35(2–3), 551–566, doi:*10.1007/s00382-009-0708-3*.

Schmitt, R. (2008), Salinity and the global water cycle, Oceanography, 21(1), 12–19, doi:*10.5670/oceanog.2008.63*.

Skliris, N., R. Marsh, S. A. Josey, S. A. Good, C. Liu, and R. P. Allan (2014), Salinity changes in the World Ocean since 1950 in relation to changing surface freshwater fluxes, Clim. Dyn., 43(3–4), 709–736, doi:*10.1007/s00382-014-2131-7*.

Steele, M., and W. Ermold (2007), Steric sea level change in the Northern Seas, J. Clim., 20(3), 403–417, doi:*10.1175/JCLI4022.1*.

Stendardo, I., M. Rhein, and R. Hollmann (2016), A high resolution salinity time series 1993–2012 in the North Atlantic from Argo and Altimeter data, J. Geophys. Res. Oceans, 121, 2523–2551, doi:*10.1002/2015JC011439*.

Stott, P. A., R. T. Sutton, and D. M. Smith (2008), Detection and attribution of Atlantic salinity changes, Geophys. Res. Lett., 35, L21702, doi:*10.1029/2008GL035874*.

Stouffer, R., et al. (2006), Investigating the causes of the response of the thermohaline circulation to past and future climate changes, J. Clim., 19(8), 1365–1387.

Terray, L., L. Corre, S. Cravatte, T. Delcroix, G. Reverdin, and A. Ribes (2012), Near-surface salinity as nature's rain gauge to detect human influence on the tropical water cycle, J. Clim., 25(3), 958–977, doi:*10.1175/JCLI-D-10-05025.1*.

Ting, M., Y. Kushnir, R. Seager, and C. Li (2011), Robust features of Atlantic multi-decadal variability and its climate impacts, Geophys. Res. Lett., 38, L17705, doi:*10.1029/2011GL048712*.

Trenberth, K. E., et al. (2007), Observations: Atmospheric surface and climate change, in Climate Change 2007: The Physical Science Basis, pp. 235–336, Cambridge Univ. Press, Cambridge, U. K., and New York.

Vellinga, M., and P. Wu (2004), Low-latitude freshwater influence on centennial variability of the atlantic thermohaline circulation, J. Clim., 17(23), 4498–4511, doi:*10.1175/3219.1*.

Vinogradova, N. T., and R. M. Ponte (2013), Clarifying the link between surface salinity and freshwater fluxes on monthly to interannual time scales, J. Geophys. Res. Oceans, 118, 3190–3201, doi:*10.1002/jgrc.20200*.

Visbeck, M., E. P. Chassignet, R. G. Curry, T. L. Delworth, R. R. Dickson, and G. Krahmann (2003), The ocean's response to North Atlantic Oscillation variability, in The North Atlantic Oscillation: Climatic Significance and Environmental Impact, edited by J. W. Hurrell et al., pp. 113–145, AGU, Washington, D. C, doi:*10.1029/134GM06*.

Wang, C., S. Dong, and E. Munoz (2010), Seawater density variations in the North Atlantic and the Atlantic meridional overturning circulation, Clim. Dyn., 34(7–8), 953–968, doi:*10.1007/s00382-009-0560-5*.

Yang, Q., T. H. Dixon, P. G. Myers, J. Bonin, D. Chambers, and M. R. van den Broeke (2016), Recent increases in Arctic freshwater flux affects Labrador Sea convection and Atlantic overturning circulation, Nat. Commun., 7, 10525, doi:*10.1038/ncomms10525*.

Yu, L. (2010), On sea surface salinity skin effect induced by evaporation and implications for remote sensing of ocean salinity, J. Phys. Oceanogr., 40(1), 85–102, doi:*10.1175/2009JPO4168.1*.

Yu, L. (2011), A global relationship between the ocean water cycle and near-surface salinity, J. Geophys. Res., 116, C10025, doi:*10.1029/2010JC006937*.

Zhang, R., and T. L. Delworth (2006), Impact of Atlantic multidecadal oscillations on India/Sahel rainfall and Atlantic hurricanes, Geophys. Res. Lett., 33, L17712, doi:*10.1029/2006GL026267*.

Zhang, R., et al. (2013), Have aerosols caused the observed Atlantic multidecadal variability?, J. Atmos. Sci., 70(4), 1135–1144, doi:*10.1175/JAS-D-12-0331.1*.

Figures

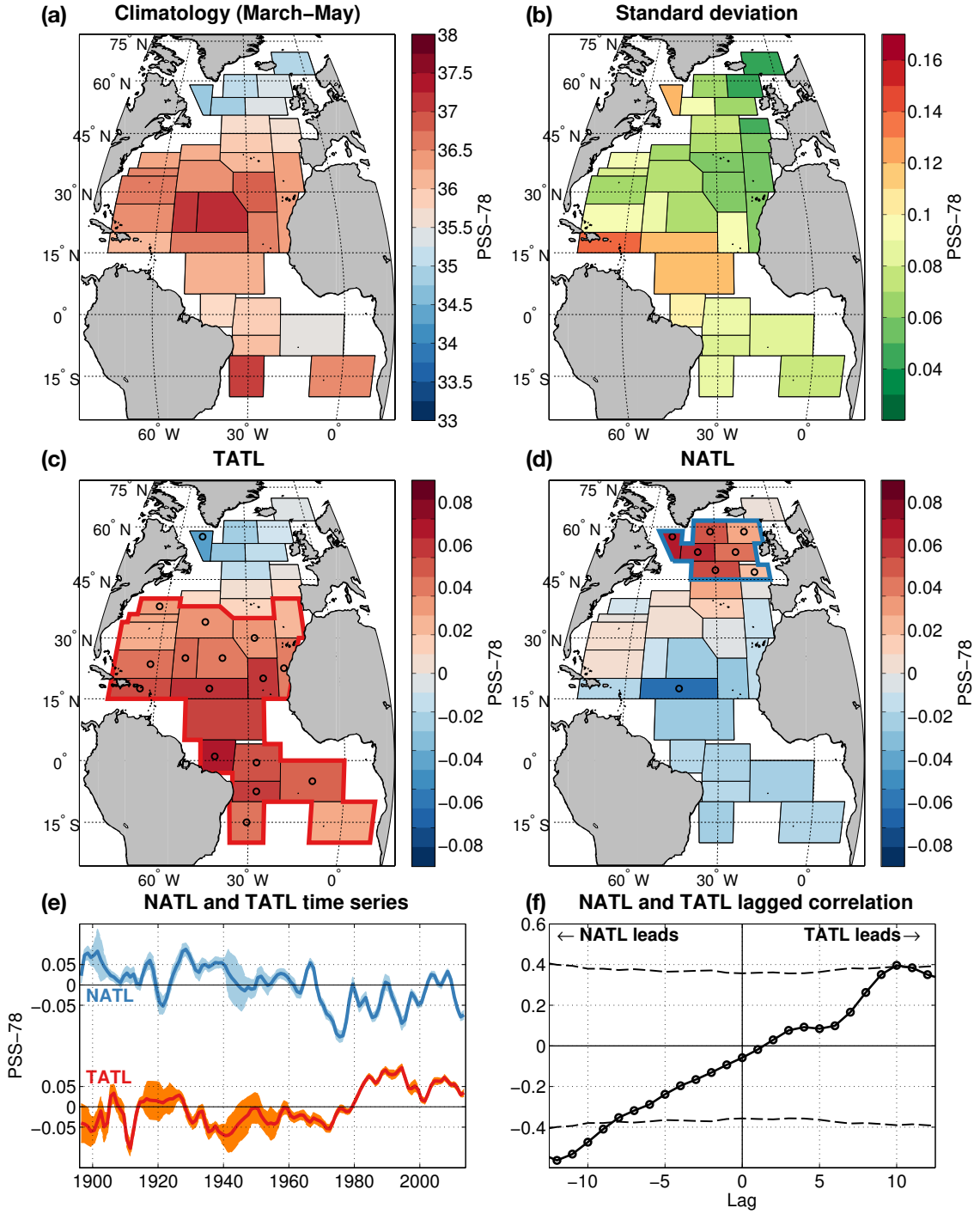

Figure 1. (a) Mean SSS climatology (March–May), in PSS-78. (b) SSS standard deviation, in PSS-78. (c) TATL (area-averaged SSS from 20°S–40°N) spatial pattern shown as the slope of SSS regressed onto the normalized TATL time series, in PSS-78. The circles indicate where the correlation with TATL is significant at $p < 0.05$. The red solid outline indicates the TATL region. (d) Same as Figure 1c but for NATL (45°–62°N). The blue solid outline indicates the NATL region. (e) NATL (top) and TATL (bottom) time series, in PSS-78. Shading indicates ±2 standard error terms. (f) Lagged correlation of NATL and TATL. The dashed lines show the 95% CIs.

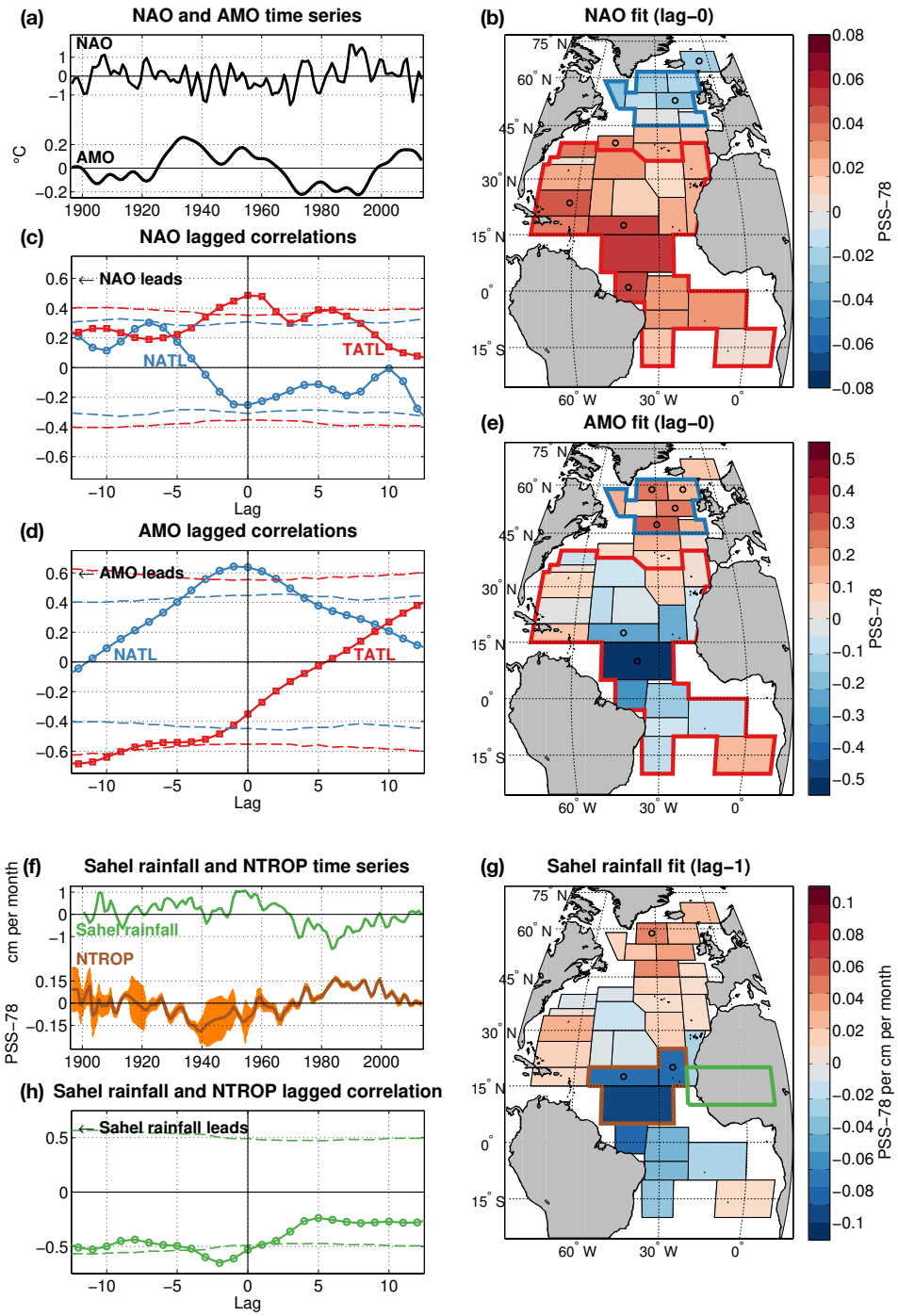

Fig. 2: (a) top: NAO index, in normalized units; bottom: AMO index, in °C. (b) Lag − 0 fit of detrended SSS versus the NAO, in PSS-78. The circles indicate where the correlation is significant at $p < 0.05$. Lagged correlations of the (c) NAO and (d) AMO and NATL (blue circles) and TATL (red squares). The dashed lines show the 95% CIs. (e) Same as Figure 2b but for the AMO, in PSS-78 per °C. (f) top: Sahel rainfall anomaly, in cm per month. Bottom: area-averaged SSS anomalies from 55° to 20°W, 5° to 20°N (NTROP), in PSS-78. Shading indicates ±2 standard error terms. (g) Lag − 1 fit of detrended SSS versus Sahel rainfall, in PSS-78 per cm per month. The circles indicate where the correlation is significant at $p < 0.05$. The NTROP and Sahel rainfall regions are outlined in orange and green respectively. (h) Lagged correlations of NTROP with Sahel rainfall. The dashed lines show the 95% CIs.

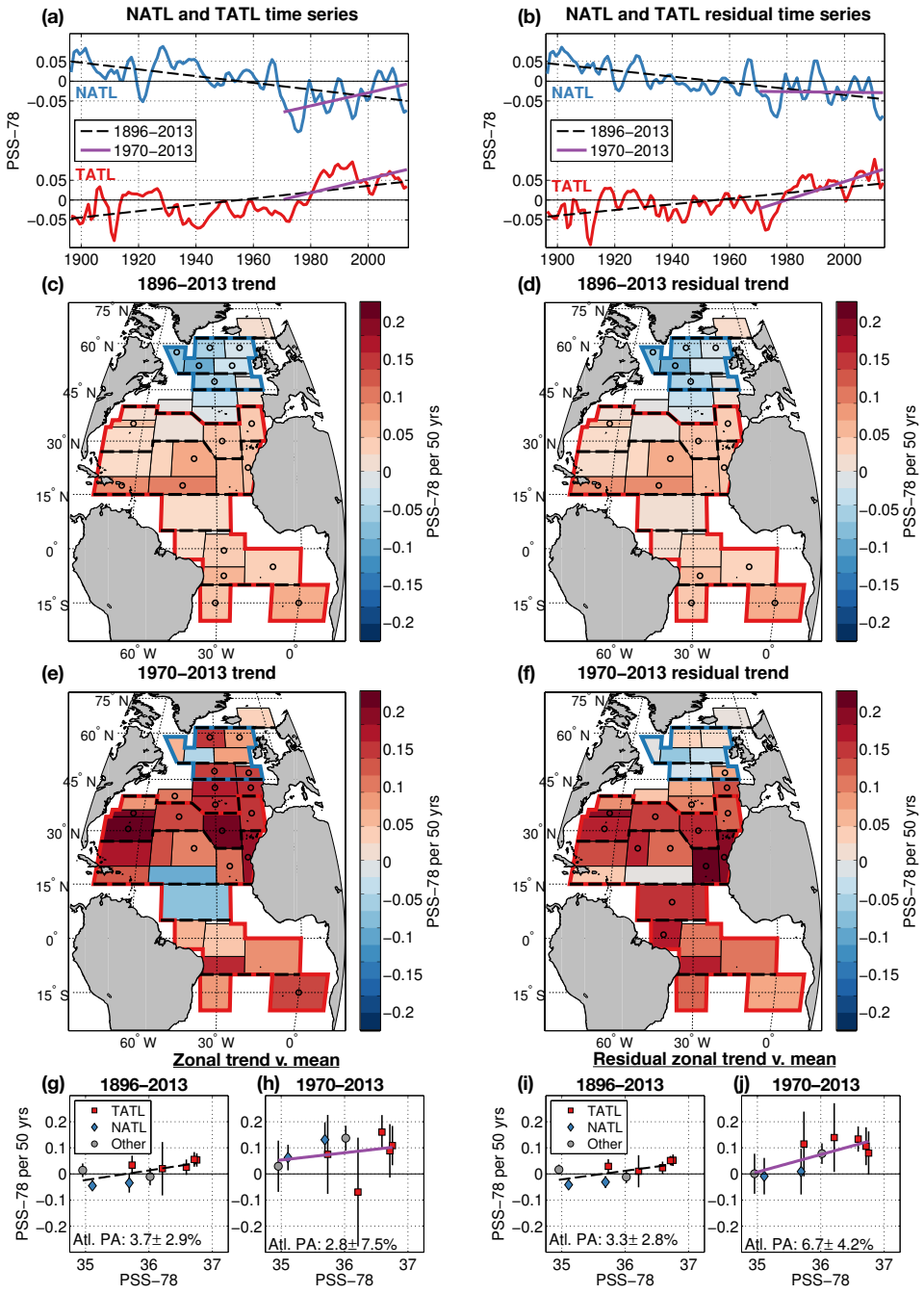

Figure 3: NATL (top) and TATL (bottom) time series for the (a) original and (b) multiple regression residual SSS, in PSS-78. The 1896–2013 (dashed black) and 1970–2013 (solid purple) trends are indicated. The 1896–2013 SSS trends for the (c) original and (d) residual SSS, in PSS-78 per 50 years. The circles indicate where the slope is significant at $p < 0.05$. (e and f) Same as Figures 3c and 3d but for the 1970–2013 trends. (g) Area-averaged zonal SSS trends from Figure 3a versus zonal mean climatology from Figure 1a. Zonal regions are indicated by dashed lines in Figure 3c. The red squares and blue diamonds indicate TATL and NATL respectively; other regions are indicated by grey circles. Error bars indicate the 95% CIs of the regression slopes. The dashed line shows the Atlantic PA coefficient, which is indicated at bottom. (h) Same as Figure 3g but using the 1970–2013 trends from Figure 3e. (i and j) Same as Figures 3g and 3h but using the 1896–2013 residual trends from Figure 3d and the 1970–2013 residual trends from Figure 3f.